Smart Mater. Struct. **20** (2011) 125013 (11pp) doi:10.1088/0964-1726/20/12/125013

Underwater thrust and power generation using flexible piezoelectric composites: an experimental investigation toward self-powered swimmer-sensor platforms

Alper Erturk[1] **and Ghislain Delporte**[2]

[1] G W Woodruff School of Mechanical Engineering, Georgia Institute of Technology, Atlanta, GA 30332-0405, USA
[2] Institut Catholique d'Arts et Métiers, 59800 Lille, France

E-mail: alper.erturk@me.gatech.edu

Received 19 June 2011, in final form 21 October 2011
Published 28 November 2011
Online at stacks.iop.org/SMS/20/125013

Abstract
Fiber-based flexible piezoelectric composites offer several advantages to use in energy harvesting and biomimetic locomotion. These advantages include ease of application, high power density, effective bending actuation, silent operation over a range of frequencies, and light weight. Piezoelectric materials exhibit the well-known direct and converse piezoelectric effects. The direct piezoelectric effect has received growing attention for low-power generation to use in wireless electronic applications while the converse piezoelectric effect constitutes an alternative to replace the conventional actuators used in biomimetic locomotion. In this paper, underwater thrust and electricity generation are investigated experimentally by focusing on biomimetic structures with macro-fiber composite piezoelectrics. Fish-like bimorph configurations with and without a passive caudal fin (tail) are fabricated and compared. The favorable effect of having a passive caudal fin on the frequency bandwidth is reported. The presence of a passive caudal fin is observed to bring the second bending mode close to the first one, yielding a wideband behavior in thrust generation. The same smart fish configuration is tested for underwater piezoelectric power generation in response to harmonic excitation from its head. Resonant piezohydroelastic actuation is reported to generate milli-newton level hydrodynamic thrust using milli-watt level actuation power input. The average actuation power requirement for generating a mean thrust of 19 mN at 6 Hz using a 10 g piezoelastic fish with a caudal fin is measured as 120 mW. This work also discusses the feasibility of thrust generation using the harvested energy toward enabling self-powered swimmer-sensor platforms with comparisons based on the capacity levels of structural thin-film battery layers as well as harvested solar and vibrational energy.

(Some figures may appear in colour only in the online journal)

1. Introduction

The interdisciplinary research fields of biomimetic locomotion and energy harvesting have independently received growing attention over the last decade. Some of the end applications of aquatic locomotion using biomimetic systems include various autonomous underwater vehicle missions, underwater exploration for sustainable ecology, mining, archeology, drug delivery, and disease screening in medicine [1–17]. The goal in the field of vibration-based energy harvesting is to enable self-powered electronic components, such as wireless sensor networks, by converting the waste vibrational energy available in their environment into electricity so that the need for an external power source and the chemical waste of conventional batteries can be minimized [18–32].

In 1926, Breder [33] divided the basic swimming modes of fish into two parts based on the propulsive structure being used: body and/or caudal fin (BCF) locomotion and median and/or paired fin (MPF) locomotion. MPF locomotion is generally employed at slow speeds, offering greater maneuverability and propulsive efficiency while BCF locomotion can achieve greater thrust and accelerations [33]. For its ease of realization and effectiveness in thrust generation, BCF locomotion [33–35] has been heavily researched in aquatic biorobotics [1–17]. Due to their silent operation, ease of fabrication, ease of application, and scalability, smart materials such as ionic polymer–metal composites (IPMCs) [4–7], shape-memory alloys (SMAs) [8–10], and fiber-based piezoelectric composites [11, 12] have attracted growing interest for biomimetic locomotion (as compared to the use of conventional actuators [13–17], such as hydraulic actuators or servomotors combined with gear trains, cranks, or mechanisms). As pointed out by Lauder *et al* [36] in a recent article, smart materials can be used for testing the hypotheses of experimental biologists [36–40], such as the effect of active stiffness in undulatory self-propulsion [36] or the contribution of various fins and body parts to thrust generation [37].

As proposed by Williams and Yates [18] in their early paper on vibration-based energy harvesting, the basic transduction mechanisms that can be used for vibration-to-electricity conversion are the electromagnetic [18–20], electrostatic [21, 22], and piezoelectric [23–25] transduction methods. Other techniques of vibration-based energy harvesting include magnetostriction [26, 27] and the use of electroactive polymers (EAPs) [28–30]. Among these alternatives, piezoelectric materials have been most widely studied over the past decade [23, 24] due to their large power density and ease of application. Voltage outputs in electromagnetic, magnetostrictive, and EAP-based energy harvesting methods are typically very low and often multi-stage post-processing is required in order to reach a voltage level that can charge a storage component. In piezoelectric energy harvesting, however, usable voltage outputs can be obtained directly from the piezoelectric material itself. When it comes to electrostatic energy harvesting, an input voltage or charge needs to be applied so that the relative vibratory motion of the capacitor elements creates an alternating electrical output. The voltage output in piezoelectric energy harvesting emerges from the constitutive behavior of the material, which eliminates the requirement of an external voltage input. Moreover, unlike electromagnetic devices, piezoelectric devices can be fabricated both in macro-scale and micro-scale due to the well-established thick-film and thin-film fabrication techniques [31, 32]. Poor properties of planar magnets and the limited number of turns that can be achieved using planar coils are some of the main practical limitations in enabling micro-scale electromagnetic energy harvesters [24].

Based on the existing literature, it can be inferred that piezoelectric materials offer many advantages to use in bio-inspired robotics and energy harvesting as well as in their combined future applications, such as the ultimate concept of self-powered swimmer-sensor platforms. Fiber-based piezoelectric composites, particularly the macro-fiber composites (MFCs) [41, 42] developed at NASA within the past decade, constitute a structurally flexible option as an effective bending actuator and power generator. Although the advantages of piezoelectric transduction over some of the alternatives (such as conventional servomotors) are evident, it is worth highlighting that piezoelectric materials have certain advantages over the closest alternatives as well. For instance, as another type of smart material, IPMCs are very convenient for low-frequency thrust generation using low-voltage inputs [4–7]; however, they are not as effective power generators as piezoelectric materials (with reported power outputs below nano-watts [30]). Using piezoelectric transduction, both low-frequency and high-frequency actuation are possible in biomimetic locomotion (through the converse piezoelectric effect) and high power density levels are obtained in energy harvesting (through the direct piezoelectric effect). Table 1 summarizes the advantages of MFC piezoelectric structures for underwater thrust and power generation. Possibly the only disadvantage of MFCs is their relatively high-voltage requirement in actuation, which is associated with very low current and which becomes an advantage in reverse operation for energy harvesting to charge a storage device (high-voltage output is obtained without any voltage multiplier circuit). Moreover, small-size amplifiers (for converting battery voltage levels to kV level) are available off the shelf for actuation.

Table 1. Main advantages of flexible MFC piezoelectric structures for underwater thrust and power generation.

Advantages for thrust generation	Advantages for power generation
• Ease of fabrication and application	• Ease of fabrication and application
• Efficient bending actuation (33-mode)	• High power density
• Silent operation	• No external bias voltage input requirement
• Both low-frequency and high-frequency operation	• No voltage multiplier requirement (high voltage is extracted directly)

This paper aims to combine the research fields of biomimetic locomotion and energy harvesting through the concept of *piezohydroelasticity* toward enabling a power generator—swimmer *smart fish* for underwater robotics and sensing applications. As far as the thrust generation mechanism is concerned, carangiform-type BCF locomotion is considered for its simplicity and effectiveness in thrust generation. In the following, the focus is first placed on thrust generation by underwater piezoelectric actuation. Details of the experimental setup and its calibration for thrust measurement are presented. Two bimorph fish samples are fabricated (with and without a passive caudal fin) and compared in terms of their thrust frequency response functions (FRFs). The configuration with a passive caudal fin is further investigated for its power generation performance. Finally, the feasibility of thrust generation using the harvested solar and vibrational energy is discussed.

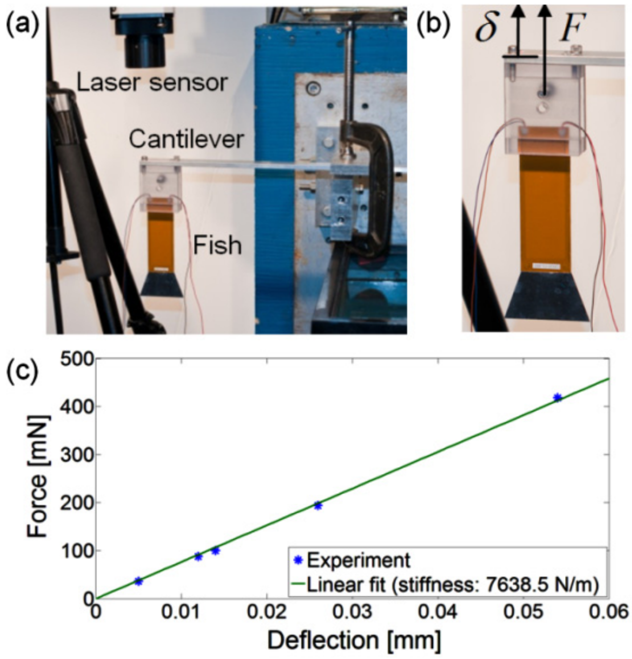

Figure 1. (a) Calibration of the setup to obtain the force–deflection relation in the presence of a fish sample and its clamp; (b) close-up view showing the point of applied calibration loads (F) at the head of the fish and the point of deflection (δ) measurement; (c) linear calibration curve with the identified linear stiffness (F/δ) value.

2. Underwater thrust generation by piezoelectric actuation

2.1. Calibration of the thrust measurement setup

Hydrodynamic thrust measurement under piezoelectric actuation is a more involved task as compared to measurements of the dynamic kinematic variables, such as velocity and acceleration. The reason is that the thrust output is a one-directional force resultant achieved during the oscillatory actuation of the piezoelastic structure at steady state. A 254 mm × 25.4 mm × 6.35 mm aluminum cantilever is combined with a laser sensor to obtain an elastic transducer for this purpose. The fish sample with its plexiglass clamp is attached to the tip of the horizontally located *transducer cantilever* as shown in figure 1(a). A set of small masses are then gradually located at the center of the fish head to emulate the force (thrust) by the help of gravity. The resulting deflection is recorded by the laser sensor (figure 1(b)) and eventually the linear calibration curve shown in figure 1(c) is obtained. Note that the transducer cantilever responds linearly up to several hundreds of milli-newtons and the decoder of the laser sensor is sensitive enough to capture the resulting deflection amplitudes.

2.2. Underwater actuation and thrust measurement

After the calibration curve of the transducer cantilever is obtained in air, the transducer cantilever with a clamped fish sample is immersed in water for the hydrodynamic thrust measurements using the experimental setup shown in figure 2.

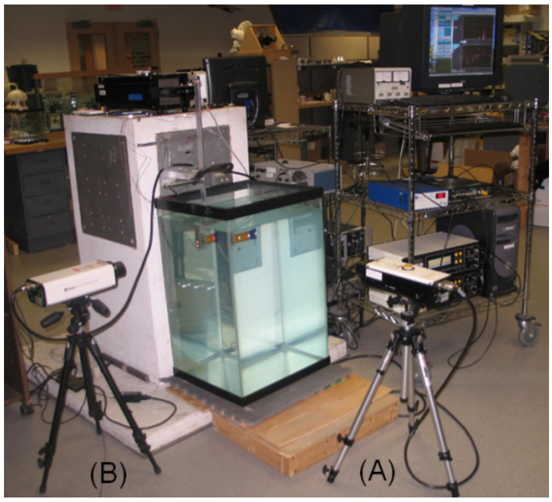

Figure 2. Experimental setup used for underwater thrust measurement after the transducer cantilever with a clamped fish sample is immersed in water. Laser A is used for obtaining the transverse tail velocity-to-actuation voltage input FRFs whereas laser B is used to measure the mean head displacement during the manual frequency sweep for evaluating the hydrodynamic thrust.

It is important to note that the dimensions of the transducer cantilever are such that its underwater fundamental resonance frequency is sufficiently higher than the underwater actuation frequencies of interest (this is checked by impact hammer testing of the transducer cantilever). Hence, one is in the quasi-static region of the transducer cantilever in the thrust generation experiments and the tip deflection of the cantilever is due to the dynamics of the fish sample only (i.e. there is no interaction with the dynamics of the transducer cantilever). In addition, the hydrostatic pressure distributions on both faces of the transducer cantilever cancel each other so that the in-air thrust–deflection calibration is valid.

In figure 2, the laser vibrometer pointing from the transverse direction of the fish sample (laser A) is employed for extracting the modal frequencies of the fish sample (in bending) through the tail velocity-to-actuation voltage FRFs. The second laser vibrometer (laser B) measures the displacement of the transducer cantilever (as in figure 1(a)) in the perpendicular direction so that the mean displacement can be converted to thrust using the calibration curve (figure 1(c)).

Harmonic actuation is used for hydrodynamic thrust generation. The frequency increment used in the time-domain thrust measurements is 0.5 Hz. At each frequency of voltage actuation, three time-domain displacement measurements are taken (using laser B in the configuration described by figure 2): pre-actuation, actuation, and post-actuation. An example is displayed in figure 3 for the thrust measurement at 6 Hz under the peak-to-peak actuation input of 1050 V. The first measurement in this scheme is the *pre-actuation* measurement, which is simply the laser reading in the absence of piezoelectric actuation (i.e. noise around the origin). Then, the voltage actuation is started and the data are recorded after the system reaches its steady state, which is the *actuation* measurement. Finally, the actuation is stopped and a last measurement is taken in the absence of any actuation or transients. This is

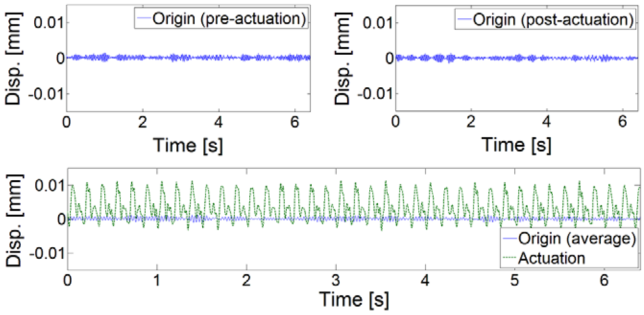

Figure 3. Displacement measurements at the head of the fish sample (in the direction of positive thrust) during pre-actuation, post-actuation, and actuation (along with the average of the pre-actuation and post-actuation histories, which defines the averaged origin).

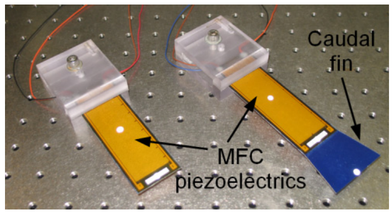

Figure 4. Bimorph fish samples without and with a passive caudal fin.

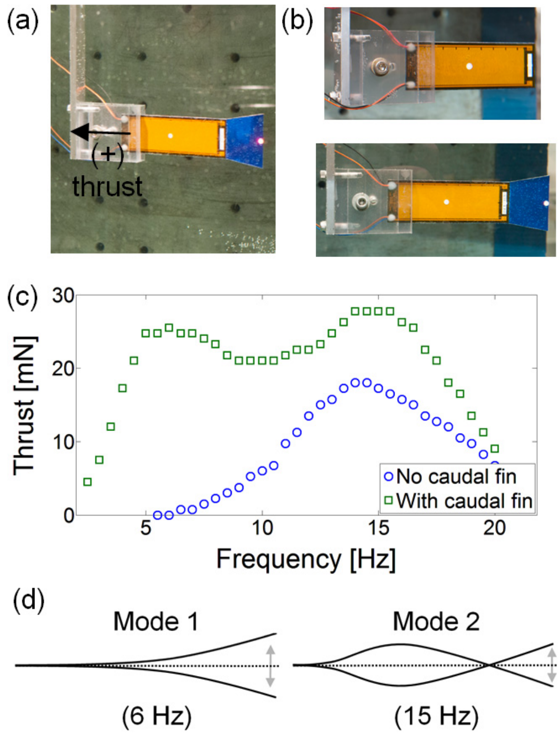

Figure 5. (a) Underwater configuration of a fish sample; (b) two fish configurations without and with a passive caudal fin; (c) comparison of thrust frequency response for the same actuation input (peak-to-peak voltage: 1050 V) showing the substantial advantage of the fish sample with a caudal fin; (d) mode shapes of the configuration with a passive caudal fin (for the neutral surface without showing the details of cross-section change due to the fin).

the *post-actuation* measurement. The origin is defined as the average of the pre-actuation and post-actuation measurements. The mean displacement caused by the thrust is the difference between the mean value of the actuation measurement and the mean value of the averaged origin measurement. This mean displacement reading is then used in figure 1(c) to give the mean thrust at the frequency of measurement. Note that the laser signal amplitude is divided by the refractive index of water ($n = 1.333$) in the underwater experiments and the validity of this signal correction is checked through another set of experiments not discussed here. Another important optical consideration when taking laser measurements through a transparent but reflective interface (clean glass in this case) is to make sure that the reflection from the interface is *not* on the lens. This is easy to realize with laser vibrometers of low numerical aperture by angling the laser sensor head slightly.

2.3. The effect of caudal fin on the thrust frequency response

Two bimorph fish samples are fabricated using a 0.127 mm thick aluminum sheet as the substrate material and MFCs as the active material (MFC-8528-P1 type from the Smart Material Corporation [42]). The active length and width of the MFC layers are 85 mm and 28 mm, respectively. The MFC layers are bonded onto both faces of the aluminum substructure using high-shear strength epoxy (3M DP460) in a vacuum bonding process. The active region of each bimorph fish is approximately 0.8 mm thick. As shown in figure 4, one of the two fish configurations has no caudal fin whereas the continuous (not pinned) aluminum substrate of the other bimorph extends outside the active region to give a passive tapered caudal fin of 35 mm length and 48 mm maximum width (at the tail tip). Each MFC layer has a free capacitance of 5.7 nF according to the manufacturer and parallel connection is employed here. Therefore a resultant *free* capacitance of 11.4 nF is expected for each unclamped fish sample based on the technical specifications. The measured capacitance values of the *clamped* fish samples (in air) are 7.4 nF and 8.6 nF for the configurations without and with a caudal fin, respectively. It is worth mentioning that these capacitance values have been observed to increase during the underwater experiments due to slight water absorption associated with long-term immersion, which is a fabrication-based limitation and is beyond the scope of this work[3].

The fish samples are attached to the transducer cantilever for the underwater thrust measurements. Figure 5(a) shows the alignment of the transducer cantilever with a bimorph fish sample attached at its tip. The underwater configurations of the two fish samples without and with a caudal fin are shown in figure 5(b). The thrust measurements are conducted for frequencies below 20 Hz (which cover the first two bending modes of the fish sample with a passive caudal fin). For the same harmonic actuation voltage input to each sample (1050 V of peak-to-peak voltage), figure 5(c) shows the thrust FRFs. The fundamental resonance frequency of the fish sample

[3] In some of its recent models, the manufacturer [42] uses polyester electrode sheets to make the MFCs relatively hydrophobic.

with no caudal fin is around 14.5 Hz and the mean thrust at this frequency is 18 mN. Remarkably, the fish sample with a tapered passive caudal fin exhibits two peaks in the frequency range of 0–20 Hz with much larger thrust output. In addition to its fundamental vibration mode around 6 Hz (the first bending mode), the fish with a passive caudal fin has its second vibration mode around 15 Hz (the second bending mode). The mean thrust readings for the sample with a passive caudal fin in figure 5(c) are 26 mN at 6 Hz (mode 1) and 28 mN at 15 Hz (mode 2). The mode shapes of this favorable configuration are shown in figure 5(d). Note that the second mode shape (at 15 Hz) has a node near the root of the caudal fin, hence an inflection point close to the head of the fish. It can be concluded from figure 5(c) that the configuration with a passive caudal fin is a *wideband thrust generator* with substantially larger and relatively flat thrust output as compared to the configuration with no caudal fin for the same dynamic actuation input. This is in agreement with the single-hinge and double-hinge analogies given by Azuma [28] in his book and their effect on the frequency range of optimal performance.

It is worth mentioning that the actuation performance for the second vibration mode can be improved by optimizing the surface coverage of the piezoelectric layers. It is known that the second mode shape (in figure 5(d)) has a *strain node* (which is simply an inflection point for a thin cantilever) near the root [43, 44]. Therefore, a significant portion of the actuation input cancels itself with the present surface coverage of the piezoelectric layers since the strain distributions on two sides of the strain node are 180° out of phase. Using segmented piezoelectric fibers and segmented electrodes [44] can improve actuation performance dramatically for swimming with the second mode shape.

2.4. The effect of actuation voltage on the thrust output

Further experiments are conducted with both fish samples to investigate the dependence of the thrust output on the actuation voltage. The operational voltage range of the MFC actuators is −500 to 1500 V and neither of these levels should be exceeded during the dynamic actuation. Therefore, the maximum peak-to-peak voltage input level without imposing any DC offset is 1000 V and this level can be increased up to the peak-to-peak level of 2000 V with sufficient DC offset (i.e. using 500 V DC offset with an oscillatory amplitude of 1000 V so that the maximum is 1500 V and the minimum is −500 V). In this work, the peak-to-peak voltage levels of 800, 1050, and 1300 V are studied and the resulting thrust frequency response curves are shown in figure 6. The thrust output increases monotonically with increasing voltage amplitude at every frequency. For all peak-to-peak actuation voltage levels shown in figure 6, the configuration with a passive caudal fin results in substantially better thrust generation performance with larger peak thrust as well as wideband behavior. At the highest actuation voltage level (1300 V peak-to-peak), mean thrust values of more than 30 mN are achieved in the frequency range of 4–17 Hz (with the peak values of 40 mN and 50 mN at the first two resonance frequencies, respectively). Note that the mass of the configuration with a passive caudal fin is only 10 g (excluding the mass of its plexiglass clamp head) yet the thrust levels are comparable to those of the biological counterparts [37].

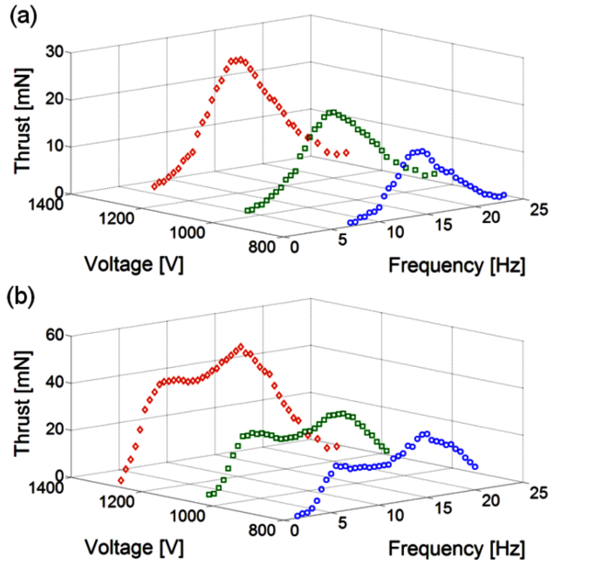

Figure 6. Variation of the thrust frequency response with peak-to-peak actuation voltage for the configurations (a) without and (b) with a caudal fin.

3. Underwater power generation using piezoelectric structures

3.1. In-air base excitation experiments for the fish sample with a caudal fin

Next, the focus is placed on the energy harvesting performance of piezoelastic fish. Although piezoelectric energy harvesting from aeroelastic vibrations has been investigated by various research groups in the past few years [45–55], there has been very limited work on the use of piezoelectric transduction for energy harvesting from hydroelastic vibrations. One particular example by Allen and Smits [56] employs a polyvinylidene fluoride (PVDF) membrane located behind a bluff body for piezoelectric power generation from the resulting von Kármán vortex street. Compared to PVDF films, the MFCs used herein offer much larger electromechanical coupling, and consequently, increased power output.

The fish sample with a passive caudal fin is first tested in air to investigate its resonant power generation performance under bending vibrations. Figure 7(a) shows the base excitation setup (base being the head of the fish) for harvesting energy from the fundamental bending mode of the sample. The fish is clamped from its head to the armature of an electromagnetic shaker. It should be noted that the in-air resonance frequencies are expected to be much higher than the underwater resonance frequencies since the added mass effect of water is not present. For linear vibrations of the fish sample (low-amplitude chirp excitation), the resistor sweep experiments are conducted to obtain the voltage output-to-base acceleration FRFs for a set of resistors ranging from the

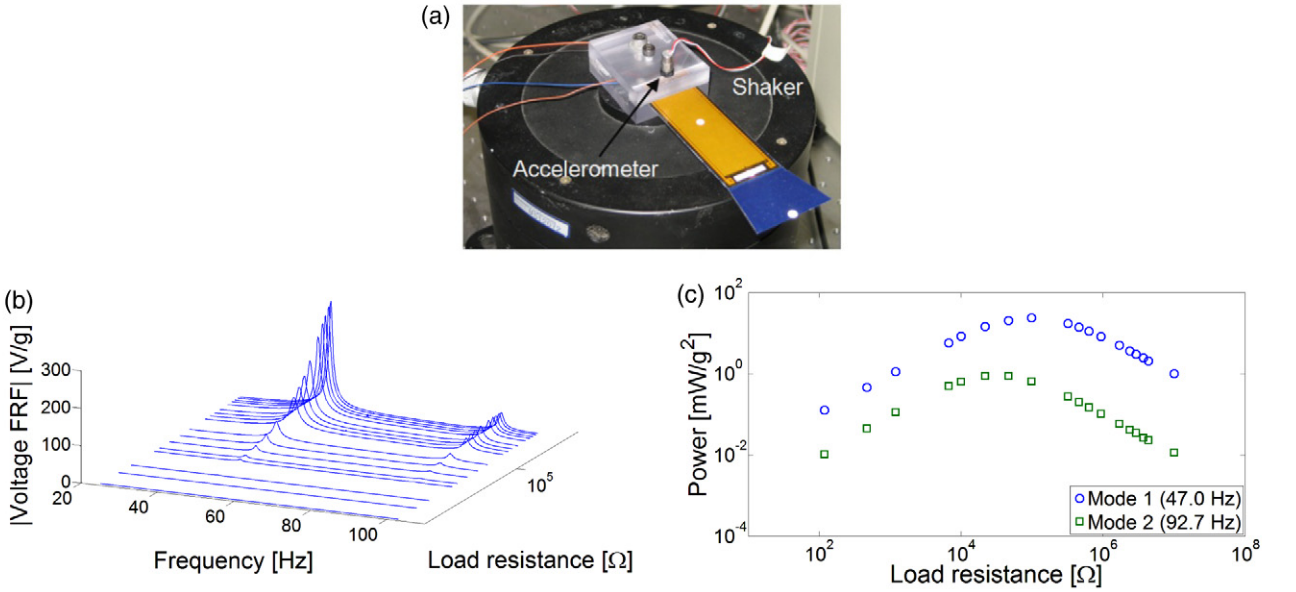

Figure 7. (a) In-air base excitation of the fish sample with a caudal fin; (b) voltage-to-base acceleration FRFs including the first two vibration modes; (c) power output versus load resistance curves for excitations at the first and the second resonance frequencies (47 and 92.7 Hz).

short-circuit to open-circuit conditions. These linear FRFs are shown in figure 7(b) and they exhibit the expected [25] trend of increasing voltage amplitude with increasing load resistance at every frequency. Note that the amplitude of the voltage output in these FRFs is given per base acceleration in *g* (gravitational acceleration) and they are valid for small acceleration inputs (usually up to a few hundred milli-*g* acceleration) so that nonlinearities (geometric, material, and dissipative) are not pronounced [57–59]. The short-circuit resonance frequencies of the first two vibration modes are 47 Hz and 92.7 Hz, respectively. The variations of the power output with load resistance for excitation at these two frequencies are plotted in figure 7(c). Expectedly, the fundamental resonance frequency (47 Hz) is of interest for the maximum power output[4]. Although the *matched resistance* is relatively high due to the low capacitance of MFCs, the maximum power amplitude is on the order of magnitude of typical monolithic (non-fiber-based) piezoelectric energy harvesters of similar dimensions. For instance, the conventional bimorph with a tip mass attachment in Erturk and Inman [60] has a peak power of 23.9 mW g^{-2} (linear estimate) for excitation at 45.6 Hz. The peak power in figure 7(c) (24.1 mW g^{-2} at 47 Hz) is indeed very much comparable to that reported in our former work [60] for a conventional bimorph cantilever[5].

[4] Recall from section 2.3 that the second vibration mode (at 92.7 Hz) has a strain node near the root [44], resulting in significant reduction of the power output around the second mode due to continuous electrodes.

[5] A common error is to assume that MFCs might be poor power generators due to their low capacitance. MFCs do have lower capacitance due to reduced electrode area (hence they typically tend to have higher matched resistance [25, 61]). However, the voltage output levels are also high due to the interdigitated electrode configuration, which is what brings the maximum power output to the same level as monolithic piezoceramics with conventional electrode coverage.

3.2. Underwater base excitation experiments for the fish sample with a caudal fin

As shown in figure 8(a), the same fish sample is connected to a seismic shaker through a stiff fixture (in an effort not to have the fixture interact with the fish modes significantly) in order to investigate piezoelectric power generation in response to underwater base excitation. The source of excitation in practice can be considered as a vibrating vehicle (such as a ship or a boat) and the fish rests attached to it from its head to harvest energy. A resistor sweep is performed for low-amplitude base excitation of the fish sample and the linear FRFs shown in figure 8(b) are obtained (the voltage amplitude is again given per base acceleration in *g*). The frequency range in figure 8(b) covers the first two vibration modes with the short-circuit resonance frequencies of 6.7 Hz and 14.5 Hz, respectively. For high acceleration levels, the linear amplitudes tend to overestimate the experimental results due to material and geometric nonlinearities as well as nonlinearities in dissipation [43, 44] (hence these linear amplitudes provide an upper bound). In particular, nonlinear fluid damping in water is expected to become effective at lower base acceleration levels as compared to in-air base excitation. Moreover, at high-excitation levels, the resonance frequencies also tend to shift from the low-excitation values in figure 8(b) (which is part of the reason that the resonance frequencies under high actuation voltage in section 2.3 are also slightly different from these values although the former is related to the converse effect)[6]. The variation of the power output with

[6] The mechanisms of nonlinear effects in actuation [62–64] and energy harvesting [57–59] can be substantially different (the former is significantly dominated by nonlinearities in coupling due to high-voltage levels). Our recent efforts [59] toward understanding the nonlinearities in energy harvesting reveal that the primary sources are the elastic (material) and dissipative nonlinearities since the electric field levels in energy harvesting are relatively low.

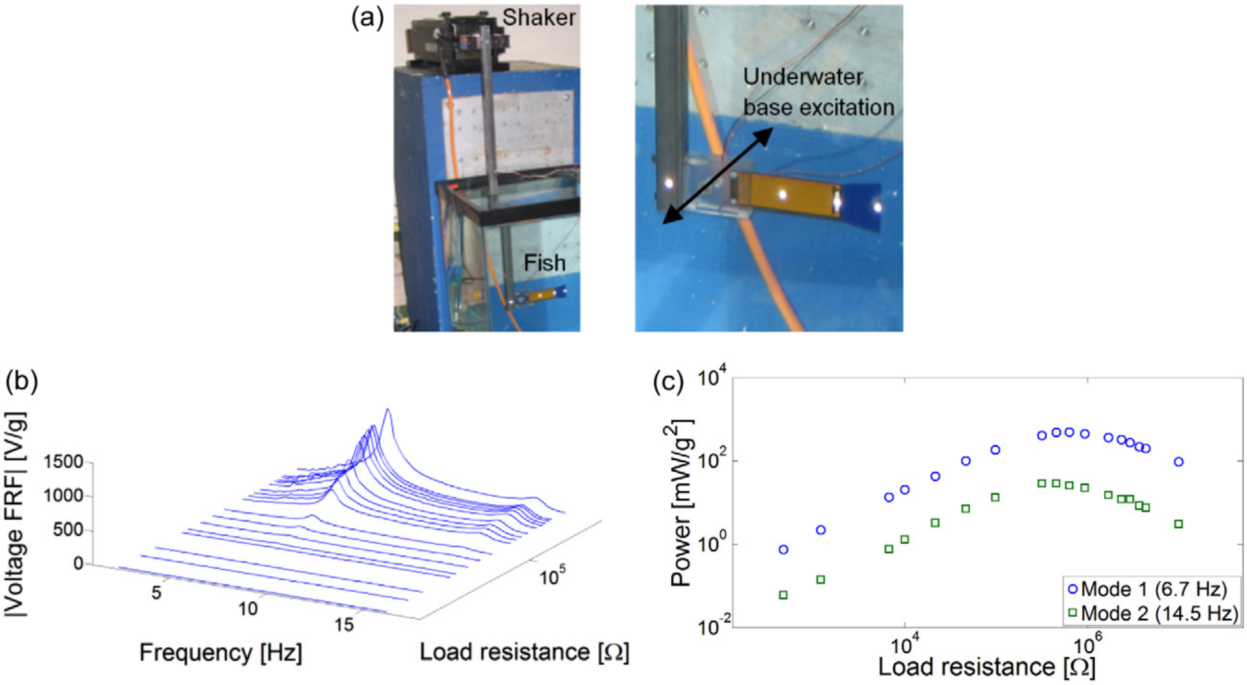

Figure 8. (a) Underwater base excitation of the fish sample with a caudal fin; (b) voltage-to-base acceleration FRFs including the first two vibration modes; (c) power output versus load resistance curves for excitations at the first and the second resonance frequencies (6.7 and 14.5 Hz).

changing load resistance for excitations at 6.7 and 14.5 Hz is plotted in figure 8(c). Once again, the fundamental mode is of primary interest for the maximum power output and the second mode response involves cancelation due to the strain node [44] of its mode shape. Comparing the in-air and underwater base excitation test results of this fish sample at the respective fundamental resonance frequencies shows that the maximum underwater power output (figure 8(c)) is an order of magnitude larger than its in-air counterpart (figure 7(c)). Hydrodynamic loads might improve the excitation amplitude for the same kinematic input from the head (base) for low-excitation levels as in figure 8. However, the dissipative effect of the surrounding fluid will also increase with increasing base excitation amplitude.

4. Toward self-powered swimmer-sensor platforms

4.1. Actuation power requirement for underwater thrust generation

A first approximation to estimate the order of magnitude of the actuation power requirement can be made through the information of capacitance and actuation voltage. Based on this approximation (using the static capacitance rather than the dynamic admittance), the electric current drawn by the actuators can be estimated as a product of the excitation frequency, actuation voltage, and capacitance. For instance, considering the fish sample with a caudal fin having the fundamental resonance frequency of around 6 Hz and static capacitance of 8.6 nF, the actuation power for 400 V input (i.e. 800 V peak-to-peak) is estimated to be around 50 mW, which gives an idea in terms of the order of magnitude. A

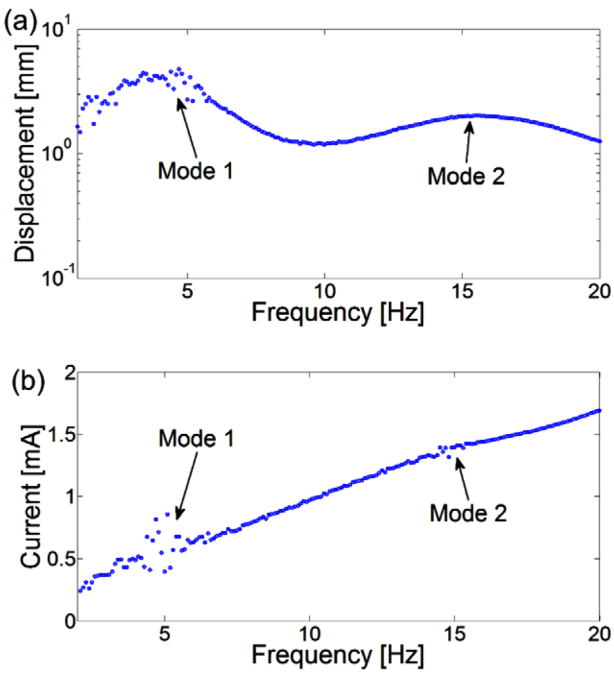

Figure 9. Variations of the (a) transverse displacement (at the MFC tip or caudal fin root) and the (b) actuation current amplitudes with frequency for the configuration with a caudal fin for 400 V actuation amplitude (peak-to-peak actuation voltage: 800 V).

better approximation requires measuring the dynamic current during the actuation through the admittance or impedance measurement at the respective excitation level. Figure 9 shows the measurements associated with the forward frequency sweep of the fish sample with a caudal fin for 400 V actuation input (800 V peak-to-peak). The first two bending modes that result in high thrust levels (recall the thrust FRF in figure 6(b) for this voltage level) can be seen in figure 9(a), which is the transverse displacement at the tip of the MFC actuators (i.e. at the root of the caudal fin). The electric current drawn by the actuators (combined in parallel) is shown in figure 9(b), where the information of the vibration modes is present (which is the information that the static capacitance estimate excludes). The current amplitude for the fundamental mode is around 0.6 mA, yielding the power amplitude of 240 mW (which gives the average power value of 120 mW)[7]. Therefore, in terms of the order of magnitude, the actuation current drawn by the MFCs at these frequencies and for these voltage levels is on the order of hundreds of micro-amps. As a result, the actuation power is on the order of hundreds of milli-watts. Note that the power consumption here refers to the actuation power only and it excludes the power requirement for any interfacing electronics between the battery and the actuators (for voltage conversion).

4.2. On the feasibility of swimming with harvested energy

Having estimated the actuation power consumed in underwater thrust generation, the feasibility of enabling self-powered swimmers that use the harvested ambient energy is discussed in this section. The sources of mechanical energy include the energy of hydrodynamic loads, vibrating ships, submarines, and boats as well as vortex streets formed behind other swimming or stationary bodies. As far as the harvesting of vibrational energy using the piezoelectric layers is concerned, it is known from our previous work [65, 66] that storing energy in the 'mAh' capacity level can take *several hours* under reasonable vibration levels[8]. Consequently, in order to store the energy that will create useful thrust for a few minutes, the fish would have to harvest vibrational energy for several hours. In practice, however, there might be applications for a short-term swimming mission of the fish and it can harvest energy for several hours (and maybe for days) before the mission. Another alternative is to use flexible solar panels as the outermost structural layers to harvest solar energy at the water surface or completely outside the water before its use. For instance, figure 10(a) shows the setup used in our recent experiments [66] for harvesting in-air solar and vibrational energy using flexible solar, piezoelectric, and thin-film battery layers. One of the two thin-film battery layers (2.5 mAh, 4 V) used as an inner layer of this composite structure is depicted in figure 10(b). A detailed schematic of the thin multifunctional structure is shown in figure 10(c). Charging of a thin-film battery layer using the solar energy is shown in figure 10(d), where the surface irradiance level of 223 W m^{-2} (created by a solar spectrum lamp) is sufficient to charge 1.3 mAh of a single battery layer in 26 min using a single flexible solar layer (figure 10(a)) of 93 mm × 25 mm surface area. Figure 10(e) shows that charging only 0.125 mAh of the same battery takes one hour using vibrational energy (under harmonic base excitation of 0.5g at 56 Hz).

Table 2. Durations of solar and vibrational energy harvesting requirement to charge 2.5 mAh of a thin-film battery layer (figure 10(b)) by extrapolating the results in Gambier *et al* [66] and the duration of thrust generation with this stored energy based on the discussion given in section 4.1 (for the ideal scenario that considers the power consumption in actuation only).

	Duration	Source/input
Solar energy harvesting	50 min	Surface irradiance and area: 223 W m^{-2} and 93 mm × 25 mm (in air)
Vibrational energy harvesting	20 h	Vibration input: 0.5g at 56 Hz (in air)
Thrust generation using the harvested energy	5 min	RMS current: 0.424 mA RMS voltage: 283 V (@ 6 Hz) mean thrust: 19 mN fish mass: 10 g (excluding the plexiglass head clamp)

The main advantages of using thin-film batteries in energy harvesting are due to their light weight and structural flexibility [65]. As far as the particular concept discussed in this paper is concerned, thin-film batteries can be used as load-bearing laminates of the fish structure in order to reduce the weight and improve the performance. Flexible solar layers can be used as the outermost layers of the fish to harvest solar energy when the fish is at the surface or outside the water. Table 2 summarizes the durations of fully charging the 50.8 mm × 25.4 mm × 0.017 mm thin-film battery layer shown in figure 10(b) (full capacity: 2.5 mAh) estimated by extrapolating the results of our charge–discharge measurements [66]. Solar energy with a flexible panel of 93 mm×25 mm can fully charge the battery in less than an hour (in air) whereas it takes several hours using the piezoelectric power output for a reasonable vibration input. Considering the discharge voltage level of the battery (4 V), 2.5 mAh full capacity provides the required average actuation power of 120 mW for 5 min (excluding the power requirement for the interface between the battery and the piezoelectric actuators).

5. Conclusions

This work experimentally investigates the concept of piezohydroelasticity for underwater thrust and power generation. Both topics (underwater locomotion and energy harvesting) are of growing interest for their independent applications of enabling bio-inspired aquatic robots and self-sustained sensor systems as well as for their combined future applications, such as the concept of self-powered swimmer-sensor platforms.

The frequency- and voltage-dependent performance of hydrodynamic thrust generation is compared under piezoelectric actuation for bimorph smart fish configurations fabricated with and without a passive caudal fin (as a

[7] Recall also that the capacitance of the MFCs discussed in this paper increases after they are immersed in water as they are not fully hydrophobic in the absence of any special coating.

[8] When performing an experiment to charge a battery by using the harvested energy, it is essential to check the discharge curve [65, 66] since plotting the voltage associated with charging alone [67, 68] can be misleading in respect of the amount of charge received by the battery.

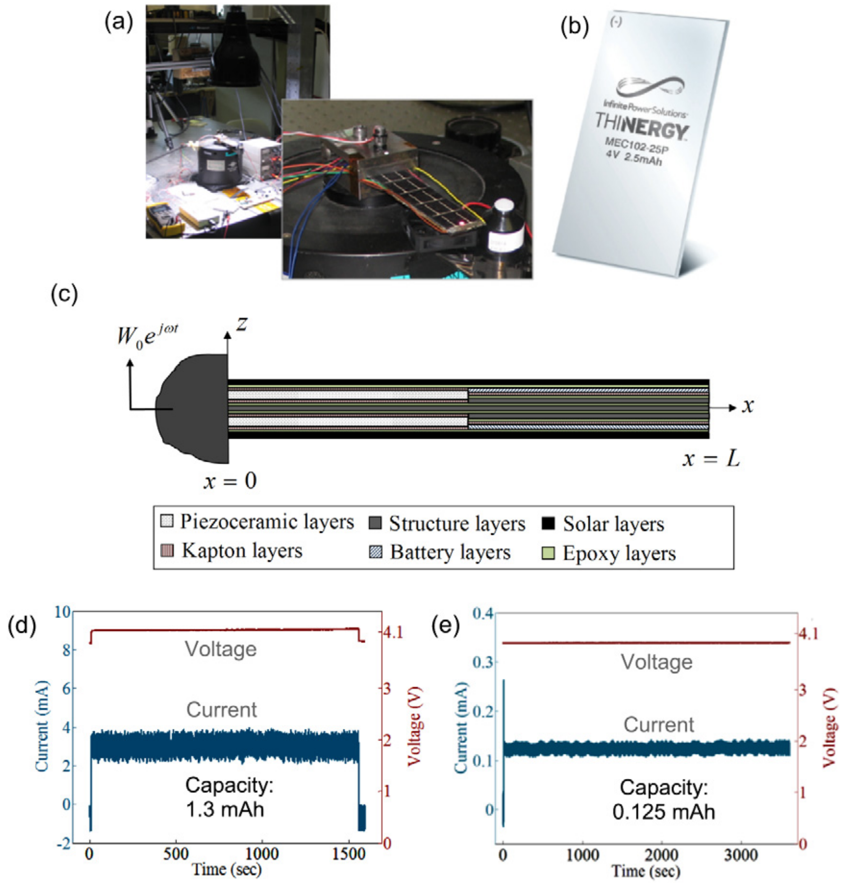

Figure 10. (a) Cantilevered flexible solar and vibrational energy harvester with two thin-film battery layers (surface area: 93 mm × 25 mm); (b) 50.8 mm × 25.4 mm × 0.017 mm battery layer used as an inner layer (Thinergy MEC102, Infinite Power Solutions, Inc.; 2.5 mAh, 4 V [69]); (c) schematic of the multifunctional structure; (d) charging of a battery layer using the top solar panel (surface irradiance level: 223 W m^{-2}); (e) charging of a battery layer using the combined output of two piezoelectric layers (base excitation: 0.5g at 56 Hz).

continuous extension of the substrate material). The favorable effect of having a passive caudal fin on the frequency bandwidth of thrust generation is reported. It is concluded that the passive caudal fin brings the second vibration mode close to the first one and makes the smart fish a wideband thrust generator (as well as a wideband power generator). The effect of actuation voltage on the thrust output is also investigated for the fish configuration with a passive caudal fin (which has a mass of 10 g excluding its clamp head). For the highest actuation voltage level (1300 V peak-to-peak), mean thrust values of more than 30 mN are obtained in the frequency range of 4–17 Hz (with the peak values of 40 mN and 50 mN at the first two resonance frequencies, respectively). Underwater base excitation of the smart fish (from its head) is also performed for piezoelectric power generation.

Finally, the feasibility of thrust generation using the harvested energy is discussed briefly based on the actuation current and voltage measurements. The average power requirement for generating a mean thrust of 19 mN at 6 Hz is measured as 120 mW. A 50.8 mm × 25.4 mm × 0.017 mm thin-film battery (2.5 mAh, 4 V) can provide this power for 5 min (ignoring the power consumption in the interfacing circuit between the battery and the actuators for voltage conversion). Such a light weight and flexible battery (which can act as a structural layer of the fish) can be charged in less than an hour using solar energy (in 50 min for an irradiance level of 223 W m^{-2}—typical in-air measurement) by means of flexible solar layers and in several hours using vibrational energy of reasonable levels (in 20 h for 0.5g base acceleration at 56 Hz—typical in-air measurement). Although the harvesting duration is substantially longer than the duration of thrust generation in the vibrational energy harvesting case, the concept can find applications for short-term swimming missions where the smart fish can harvest energy for hours or days prior to the mission.

Acknowledgments

The experiments discussed herein were conducted by the authors (AE and his visiting intern GD) in the Center for Intelligent Material Systems and Structures at Virginia Tech, AE's previous institution.

References

[1] Bandyopadhyay P R 2005 Trends in biorobotic autonomous undersea vehicles *IEEE J. Ocean. Eng.* **30** 109–39

[2] Roper D T, Sharma S, Sutton R and Culverhouse P 2011 A review of developments towards biologically inspired propulsion *Proc. Inst. Mech. Eng.* E **255** 77–96

[3] Zhang Z G, Gondo M, Yamashita N, Yamamoto A and Higuchi T 2007 Design and control of a fish-like robot using and electrostatic motor *Proc. 2007 IEEE Int. Conf. on Robotics and Automation (Rome, April 2007)*

[4] Guo S, Ge Y, Li L and Liu S 2006 Underwater swimming micro robot using IPMC actuator *Proc. 2006 IEEE Int. Conf. on Mechatronics and Automation (Luoyang, June 2006)*

[5] Peng H, Ding Q and Li H 2009 Fabrication of ionic polymer—metal composites and robot design *Front. Mech. Eng. China* **4** 332–8

[6] Chen Z, Shatara S and Tan X 2010 Modeling of biomimetic robotic fish propelled by an ionic polymer—metal composite caudal fin *IEEE/ASME Trans. Mechatronics* **15** 448–59

[7] Aureli M, Kopman V and Porfiri M 2010 Free-locomotion of underwater vehicles actuated by ionic metal polymer composites *IEEE/ASME Trans. Mechatronics* **15** 603–14

[8] Shinjo N 2005 Investigations into the use of shape memory alloy for biomimetic propulsion of underwater vehicles *PhD Thesis* Department of Marine and Environmental Systems, Florida Institute of Technology, Melbourne, FL, 260 pp

[9] Cho K, Hawkes E, Quinn C and Wood R J 2008 Design, fabrication and analysis of a body-caudal fin propulsion system for a microrobotic fish *Proc. 2008 IEEE Int. Conf. on Robotics and Automation (Pasadena, CA, May 2008)*

[10] Wang Z, Hang G, Li J, Wang Y and Xiao K 2008 A micro-robot fish with embedded SMA wire actuated flexible biomimetic fin *Sensors Actuators* A **144** 354–60

[11] Nagata Y, Park S, Ming S and Shimojo M 2008 Development of underwater robot using macro fiber composite *Proc. 2008 IEEE/ASME Int. Conf. on Advanced Intelligent Mechatronics (Xi'an, July 2008)*

[12] Ming S, Park S, Nagata Y and Shimojo M 2009 Development of underwater robots using piezoelectric fiber composite *Proc. 2009 IEEE Int. Conf. on Robotics and Automation (Kobe, May 2009)*

[13] Barrett D S 1994 The design of a flexible hull undersea vehicle propelled by an oscillator foil *MS Thesis* Department of Ocean Engineering, Massachusetts Institute of Technology, Boston, MA, 177 pp

[14] Barrett D S 1996 Propulsive efficiency of a flexible hull underwater vehicle *PhD Thesis* Department of Ocean Engineering, Massachusetts Institute of Technology, Boston, MA, 215 pp

[15] Anderson J M and Chhabra N K 2002 Maneuvering and stability performance of a robotic tuna *Integr. Compar. Biol.* **42** 118–26

[16] Low K H and Willy A 2006 Biomimetic motion planning of an undulating robotic fish fin *J. Vib. Control* **12** 1337–59

[17] Crespi A, Lachat D, Pasquier A and Ijspeert A J 2008 Controlling swimming and crawling in a fish robot using a central pattern generator *Auton. Robots* **25** 3–13

[18] Williams C B and Yates R B 1996 Analysis of a micro-electric generator for microsystems *Sensors Actuators* A **52** 8–11

[19] Glynne-Jones P, Tudor M J, Beeby S P and White N M 2004 An electromagnetic, vibration-powered generator for intelligent sensor systems *Sensors Actuators* A **110** 344–9

[20] Elvin N and Elvin A 2011 An experimentally validated electromagnetic energy harvesters *J. Sound Vib.* **330** 2314–24

[21] Mitcheson P, Miao P, Start B, Yeatman E, Holmes A and Green T 2004 MEMS electrostatic micro-power generator for low frequency operation *Sensors Actuators* A **115** 523–9

[22] Sheu G J, Yang S M and Lee T 2011 Development of a low frequency electrostatic comb-drive energy harvester compatible to SoC design by COMS process *Sensors Actuators* A **167** 70–6

[23] Anton S R and Sodano H A 2007 A review of power harvesting using piezoelectric materials (2003-2006) *Smart Mater. Struct.* **16** R1–21

[24] Cook-Chennault K A, Thambi N and Sastry A M 2008 Powering MEMS portable devices—a review of non-regenerative and regenerative power supply systems with emphasis on piezoelectric energy harvesting systems *Smart Mater. Struct.* **17** 043001

[25] Erturk A and Inman D J 2011 *Piezoelectric Energy Harvesting* (Chichester: Wiley)

[26] Wang L and Yuan F G 2008 Vibration energy harvesting by magnetostrictive material *Smart Mater. Struct.* **17** 045009

[27] Dai X, Wen Y, Li P, Yang J and Zhang G 2009 Modeling, characterization, and fabrication of vibration energy harvester using Terfenol-D/PZT/Terfenol-D composite transducer *Sensors Actuators* A **156** 350–8

[28] Koh S J A, Zhao X and Suo Z 2009 Maximal energy that can be converted by a dielectric elastomer generator *Appl. Phys. Lett.* **94** 262902

[29] Aureli M, Prince C, Porfiri M and Peterson S D 2010 Energy harvesting from base excitation of ionic polymer metal composites in fluid environments *Smart Mater. Struct.* **19** 015003

[30] Giacomello A and Porfiri M 2011 Underwater energy harvesting from a heavy flag hosting ionic polymer metal composites *J. Appl. Phys.* **109** 084903

[31] Jeon Y B, Sood R, Jeong J H and Kim S 2005 MEMS power generator with transverse mode thin film PZT *Sensors Actuators* A **122** 16–22

[32] Shen D, Park J H, Noh J H, Choe S Y, Kim S Y, Wikle H C and Kim D J 2009 Micromachined PZT cantilever based on SOI structure for low frequency vibration energy harvesting *Sensors Actuators* A **154** 103–8

[33] Breder C M 1926 The locomotion of fishes *Zoologica* **4** 159–256

[34] Sfakiotakis M, Lane D M and Davies J B C 1999 Review of fish swimming modes for aquatic locomotion *IEEE J. Ocean. Eng.* **24** 237–52

[35] Azuma A 2006 *The Biokinetics of Flying and Swimming* (Reston, VA: AIAA)

[36] Lauder G V, Madden P G A, Tangorra J L, Anderson E and Baker T V 2011 Bioinspiration from fish for smart material design and function *Smart Mater. Struct.* **20** 094014

[37] Lauder G V and Drucker E G 2002 Forces, fishes, and fluids: hydrodynamic mechanisms of aquatic locomotion *News Physiol. Sci.* **17** 235–40

[38] Lauder G V and Drucker E G 2004 Morphology and experimental hydrodynamics of fish sin control surfaces *IEEE J. Ocean. Eng.* **29** 556–71

[39] Fish F F and Lauder G V 2006 Passive and active flow control by swimming fishes and mammals *Annu. Rev. Fluid Mech.* **38** 193–224

[40] Lauder G V, Anderson E, Tangorra J L and Madden P G A 2007 Fish biorobotics: kinematics and hydrodynamics of self-propulsion *J. Exp. Biol.* **210** 2767–80

[41] High J W and Wilkie W K 2003 Method of fabricating NASA-standard macro-fiber composite piezoelectric actuators NASA/TM-2003-212427, ARL-TR-2833

[42] Smart Material Corp. (MFC supplier with the NASA standard): www.smart-material.com

[43] Crawley E F and de Luis J 1987 Use of piezoelectric actuators as elements of intelligent structures *AIAA J.* **25** 1373–85

[44] Erturk A, Tarazaga P A, Farmer J R and Inman D J 2009 Effect of strain nodes and electrode configuration on piezoelectric energy harvesting from cantilevered beams *ASME J. Vib. Acoust.* **131** 011010

[45] Bryant M and Garcia E 2009 Development of an aeroelastic vibration power harvester *Proc. SPIE* **7288** 728812
[46] Erturk A, Vieira W G R, De Marqui C Jr and Inman D J 2010 On the energy harvesting potential of piezoaeroelastic systems *Appl. Phys. Lett.* **96** 184103
[47] De Marqui C Jr, Erturk A and Inman D J 2010 Piezoaeroelastic modeling and analysis of a generator wing with continuous and segmented electrodes *J. Intell. Mater. Syst. Struct.* **21** 983–93
[48] De Marqui C Jr, Vieira W G R, Erturk A and Inman D J 2010 Modeling and analysis of piezoelectric energy harvesting from aeroelastic vibrations using the doublet-lattice method *ASME J. Vib. Acoust.* **133** 011003
[49] St Clair D, Bibo A, Sennakesavababu V R, Daqaq M F and Li G 2010 A scalable concept for micropower generation using flow-induced self-excited oscillations *Appl. Phys. Lett.* **96** 144103
[50] Tang L, Paidoussis M and Jiang J 2009 Cantilevered flexible plates in axial flow: energy transfer and the concept of flutter-mill *J. Sound Vib.* **326** 263–76
[51] Robbins W P, Morris D, Marusic I and Novak T O 2006 Wind-generated electrical energy using flexible piezoelectric materials *Proc. ASME IMECE 2006 (Chicago, IL)*
[52] Pobering S, Ebermeyer S and Schwesinger N 2009 Generation of electrical energy using short piezoelectric cantilevers in flowing media *Proc. SPIE* **7288** 728807
[53] Akaydin H D, Elvin N and Andreopoulos Y 2010 Wake of a cylinder: a paradigm for energy harvesting with piezoelectric materials *Exp. Fluids* **49** 291–304
[54] Abdelkefi A, Nayfeh A H and Hajj M R 2011 Modeling and analysis of piezoaeroelastic energy harvesters *Nonlinear Dyn.* at press (doi:10.1007/s11071-011-0035-1)
[55] Sousa V C, Anicézio M M, De Marqui C Jr and Erturk A 2011 Enhanced aeroelastic energy harvesting by exploiting combined nonlinearities: theory and experiment *Smart Mater. Struct.* **20** 094007
[56] Allen J J and Smits A J 2001 Energy harvesting eel *J. Fluids Struct.* **15** 629–40
[57] Stanton S C, Erturk A, Mann B P and Inman D J 2010 Nonlinear piezoelectricity in electroelastic energy harvesters: modeling and experimental identification *J. Appl. Phys.* **108** 074903
[58] Stanton S C, Erturk A, Mann B P and Inman D J 2010 Resonant manifestation of intrinsic nonlinearity within electroelastic micropower generators *Appl. Phys. Lett.* **97** 254101
[59] Stanton S C, Erturk A, Mann B P, Dowell E H and Inman D J 2011 Nonlinear nonconservative behavior and modeling of piezoelectric energy harvesters including proof mass effects *J. Intell. Mater. Syst. Struct.* at press
[60] Erturk A and Inman D J 2009 An experimentally validated bimorph cantilever model for piezoelectric energy harvesting from base excitations *Smart Mater. Struct.* **18** 025009
[61] Kong N, Ha D S, Erturk A and Inman D J 2010 Resistive impedance matching circuit for piezoelectric energy harvesting *J. Intell. Mater. Syst. Struct.* **21** 1293–302
[62] Crawley E and Anderson E 1990 Detailed models for piezoelectric actuation of beams *J. Intell. Mater. Syst. Struct.* **1** 4–25
[63] Crawley E and Lazarus K 1991 Induced strain actuation of isotropic and anisotropic plates *AIAA J.* **29** 944–51
[64] Tiersten H F 1993 Electroelastic equations for electrodedd thin plates subject to large driving voltages *J. Appl. Phys.* **74** 3389
[65] Anton S R, Erturk A and Inman D J 2010 Multifunctional self-charging structures using piezoceramics and thin-film batteries *Smart Mater. Struct.* **19** 115021
[66] Gambier P, Anton S R, Kong N, Erturk A and Inman D J 2010 Combined piezoelectric, solar and thermal energy harvesting for multifunctional structures with thin-film batteries *Proc. 21st Int. Conf. on Adaptive Structures and Technologies (State College, PA, October 2010)*
[67] Sodano H A, Inman D J and Park G 2005 Generation and storage of electricity from power harvesting devices *J. Intell. Mater. Syst. Struct.* **16** 67–75
[68] Sodano H A, Inman D J and Park G 2005 Comparison of piezoelectric energy harvesting devices for recharging batteries *J. Intell. Mater. Syst. Struct.* **16** 799–807
[69] Infinite Power Solutions, Inc. www.infinitepowersolutions.com